Highly Fluorescent Purine-Containing Conjugated Copolymers with Tailored Optoelectronic Properties

C. Elizabeth O'Connell,[†] Sina Sabury,[†] J. Elias Jenkins,[‡] Graham S. Collier,[§] Bobby G. Sumpter,[#] Brian K. Long,[†] and S. Michael Kilbey II[†‡*]

[†]Department of Chemistry, University of Tennessee – Knoxville, Knoxville, Tennessee 37996, United States

[‡]Department of Chemical and Biomolecular Engineering, University of Tennessee – Knoxville, Knoxville, Tennessee 37996, United States

[§]Department of Chemistry and Biochemistry, Kennesaw State University, Kennesaw, GA, 30144, United States

[#]Center for Nanophase Materials Sciences, Oak Ridge National Laboratory, Oak Ridge, Tennessee 37831, United States

* Email: mkilbey@utk.edu

KEYWORDS: purine, direct arylation polymerization, conjugated polymer, cross-conjugated, density functional theory, electronic structure, highly fluorescent

---

ABSTRACT: Conjugated copolymers containing electron donor and acceptor units in their main chain have emerged as promising materials for organic electronic devices due to their tunable optoelectronic properties. Herein, we describe the use of direct arylation polymerization to create a series of fully π-conjugated copolymers containing the highly tailorable purine scaffold as a key design element. To create efficient coupling sites, dihalopurines are flanked by alkylthiophenes to create a monomer that is readily copolymerized with a variety of conjugated comonomers, ranging from electron-donating 3,4-dihydro-2*H*-thieno[3,4-*b*][1,4]dioxepine (ProDOT) to electron-accepting 4,7-bis(5-bromo-3-hexylthiophen-2-yl)benzo[*c*][1,2,5]thiadiazole (TBTT). The comonomer choice and electronic nature of the purine scaffold allow the photophysical properties

of the purine-containing copolymers to be widely varied, with optical bandgaps ranging from 1.96 – 2.46 eV, and photoluminescent quantum yields as high as $\phi = 0.61$. Frontier orbital energy levels determined for the various copolymers by density functional theory tight binding calculations track with experimental results, and the geometric structures of the alkylthiophene-flanked purine monomer and its copolymer are nearly planar. The utility of direct arylation polymerization and intrinsic tailorability of the purine scaffold highlights the potential of these fully conjugated polymers to establish structure-property relationships based on connectivity pattern and comonomer type, which may broadly inform efforts to advance purine-containing conjugated copolymers for various applications.

■INTRODUCTION

Purines are naturally abundant materials, with adenine and guanine being perhaps the most familiar examples. While purines are routinely used in the creation of drugs or therapeutic agents, they have recently gained traction in materials applications. These efforts generally benefit from the distinctive, fused-ring heterocyclic structure of purines, which features four spatially defined sites that can be readily and specifically functionalized.[1] Computational studies of purines and their derivatives show that their electronic properties may be tailored by functionalization or expansion of the purine scaffold,[2–5] and their hydrogen bonding properties can promote molecular alignment and influence morphological organization.[2–6] The potential use of hydrogen bonding to direct or enhance the nanoscale structure in organic electronic devices has recently been explored,[7] with various researchers demonstrating the importance of purines in the molecular engineering of nucleobase-derived nanoscale materials.[8–15]

Purines are also highly fluorescent, which stimulates their use as photoactive conjugated components in the form of oligomers and small molecule "push-pull" chromophores.[16–23] In these cases, site-specific synthetic modification of the purine scaffold has been used to manipulate their optical properties, resulting in highly luminescent compounds.[16–20,24,25] Castellano and coworkers examined the impact of adding DNA or RNA bases (e.g., adenine and guanine, which are purines, as well as thymine and uracil which are pyrimidines) to the ends of π-conjugated small molecules. In those studies, telechelic small molecules were accessed by coupling nucleobases onto 2,2′:5′,2″-terthiophene (TTT) and 4,7-bis(2-thienyl)-2,1,3-benzothiadiazole (TBTT). They showed that the terminal nucleobases on these oligomers retained their ability to participate in hydrogen bonding,[25] as well as altered their frontier molecular orbital energy levels and bandgaps. The telechelic oligomers made with a TBTT core showed intramolecular charge transfer (ICT), with the purine unit acting as the electron donor and the benzothiadiazole unit acting as the electron acceptor. However, when purines were coupled to TTT, which is a good donor, no ICT was observed because the purine is not a strong enough acceptor.[20] Similarly, our recent studies of purine-containing chromophores featuring either the strong donor 4,8-bis((2-ethylhexyl)oxy)benzo[1,2-*b*:4,5-*b*′]dithiophene (BDT), the conjugated linker thiophene (T), or the strong acceptor TBTT (**Figure 1a**, top) indicated that the purine unit acts as an electron acceptor when coupled to BDT, but acts as an electron donor when coupled to TBTT.[19]

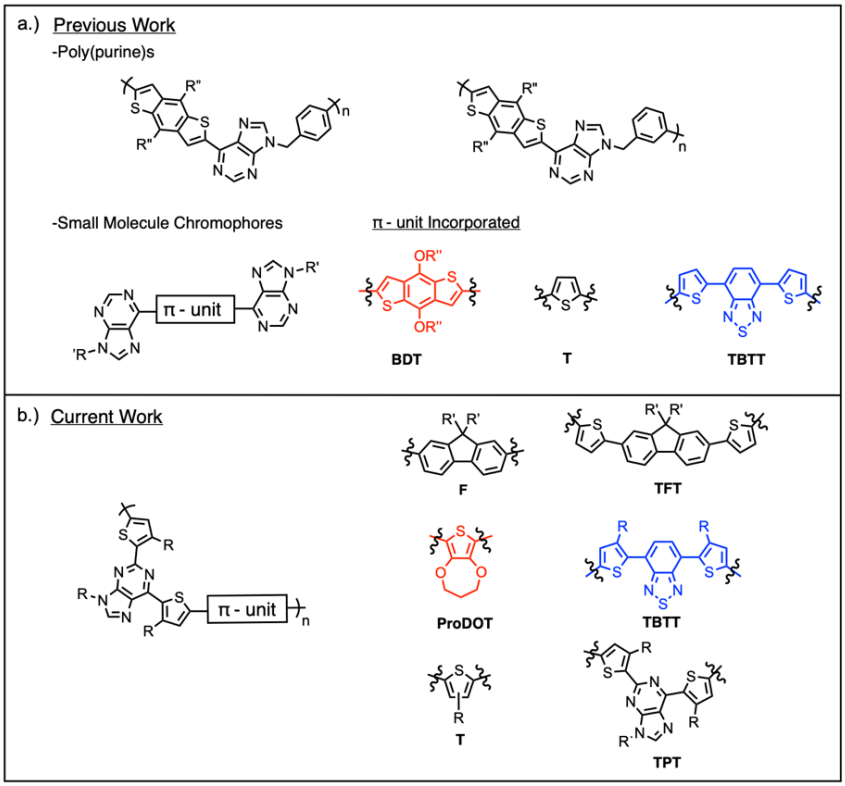

Figure 1. a) Previously reported purine-containing chromophores and copolymers, and b) conjugated purine-containing copolymers described in this work. Comonomer units are color-coded, blue for electron acceptor units, red for electron donor units, and black for linkers that extend the conjugation. In these structures R = hexyl, R' = octyl, and R" = ethylhexyl.

The impressive optoelectronic properties of purines as small molecules along with the ability of halopurines to participate in metal-mediated cross-coupling reactions,[26–28] motivated our prior efforts to synthesize polymers containing purines in the main chain.[29] In that endeavor, two different purine-containing monomers were synthesized and those dihalo-monomers were copolymerized via Stille cross-coupling polymerization with two different bis-stannane benzodithiophenes (BDT) to create purine-containing copolymers (**Figure 1a**, top). While these alternating copolymers displayed ICT, they were regiorandom, of lower molecular weight, and conjugation along their main chain was broken by the methylene unit attached at the *N*-9 position of the purine.[29]

Herein, we report the synthesis of a series of fully conjugated purine-containing copolymers that address previous issues of broken conjugation and unequal reactivity of coupling sites, and we describe the optoelectronic properties of the resulting copolymers. Because the different sites on the purine scaffold exhibit differential reactivity toward C-C bond formation by metal-mediated cross-coupling (C6 > C8 > C2),[26,27,30] a monomeric unit consisting of a purine core with flanking aromatic units that promote efficient coupling was created. Direct arylation polymerization (DArP) of the monomer triads with various conjugated comonomers allowed several π-conjugated alternating copolymers to be synthesized, as can be seen in **Figure 1b**. Complementary comonomers were selected based on their proven ability to participate in DArP and solubility in common organic solvents.[19,31–35] These copolymers displayed a range of optoelectronic properties, including decreased bandgaps due to the design of donor-acceptor conjugated polymers, high quantum yields for fluorene-containing copolymers, and fluorescent emission across a wide spectral range.

■ EXPERIMENTAL METHODS

Materials and Methods. *N*-Bromosuccinimide (NBS, 99%, Aldrich) was recrystallized from water and dried under vacuum before use. 2,6-dichloropurine (97%, Ark Pharm), 3-hexylthiophene-2-boronic acid pinacol ester (95%, Aldrich), 1-bromohexane (96%, Aldrich), glacial acetic acid, (Fisher Chemical), potassium carbonate (99%, Aldrich), $Pd(PPh_3)_4$ (98%, Aldrich), $Pd(OAc)_2$ (98%, Aldrich), pivalic acid (PivOH, 99%, Aldrich), anhydrous *N*,*N*-dimethylacetamide (DMAc, 99%, Sigma Millipore) anhydrous *N*,*N*-dimethylformamide (DMF, 99.8%, Acros Organics), anhydrous toluene (99.8%, Acros Organics), anhydrous tetrahydrofuran (THF, 99.9%, Fisher), hexanes (95%, Fisher), methanol (99%, Fisher), and chloroform (98%,

Fisher) were used as received unless stated otherwise. 3,4-Dihydro-2*H*-thieno[3,4-*b*][1,4]dioxepine (ProDOT) was synthesized according to previously published procedures.[46] Monomers and polymers were synthesized using standard Schlenk technique under an argon atmosphere.

^{13}C and ^{1}H NMR spectra of synthesized monomers were acquired at room temperature in $CDCl_3$ using a Varian VNMRS 500 MHz NMR. Time-of-flight direct analysis in real time mass spectrometry (using a JEOL AccuTOF DART mass spectrometer) was used to make high-resolution mass measurements of **M1** and **M2**. ^{1}H NMR spectra of the copolymers were acquired at room temperature in $CDCl_3$ using a Varian Mercury Vx 300 MHz NMR. Chemical shifts are referenced to residual solvent peaks. Number-average molecular weights, M_n, and dispersity, $Đ$, were determined via gel permeation chromatography (GPC). Measurements were made using an Agilent 1260 Infinity II system that used THF as the mobile phase at a flow rate of 1 mL/min at 25 °C and are reported relative to polystyrene standards. The system was equipped with a guard column and two PLgel Mixed-C columns (300 mm length) with a lower limit of 200 g/mol and an upper limit of 2×10^6 g/mol. Polymer solutions for GPC analysis were prepared at 5 mg/mL in THF and passed through a 0.2 μm PTFE filter prior to injection. Optical absorbance spectra of the copolymers and **M1** in $CHCl_3$ were acquired using a Thermo Scientific Evolution 600 spectrophotometer by scanning from 275 nm to 425 nm for **M1** and from 350 nm to 600 nm for the purine-containing copolymers. A Cary 5000 UV-Vis-NIR spectrometer was used for thin film measurements, and spectra were acquired by scanning from 350 nm to 900 nm. Beer-Lambert plots for **M1** and all copolymers were constructed from measurements of samples in $CHCl_3$, and the results are reported in **Figures S25-S31** of the *Supporting Information*. Fluorescence emission spectra were measured in $CHCl_3$ using a Cary Eclipse fluorescence spectrophotometer. Samples

were excited at the absorbance maximum of each sample and spectra were recorded by scanning from (λ_{max}^{abs} + 10) nm to 700 nm for **M1**, **P1**$_{\mathbf{TPT}}$, **P2**$_{\mathbf{F}}$, **P3**$_{\mathbf{TFT}}$, **P4**$_{\mathbf{T}}$, and **P5**$_{\mathbf{ProDOT}}$, and 850 nm for **P6**$_{\mathbf{TBTT}}$. Cyclic voltammetry was performed in acetonitrile at a scan rate of 150 mV s^{-1} using a Biological VSP3 potentiostat. Films were drop cast onto a 3 mm Au working electrode from a 1 mg/mL dichloromethane solution. The supporting electrolyte was (nBu)$_4$NPF$_6$ with Ag/AgCl as the reference electrode and a tungsten wire as the counter electrode. Thin films for optical images were painted on wax-coated paper from a $CHCl_3$ solution constituted at 1 mg/mL.

Synthesis of 2,6-dichloro-9-hexyl-9*H*-purine. A solution of 2,6-dichloropurine (5.00 g, 26.4 mmol) and potassium carbonate (9.57 g, 122 mmol) in DMF (150 mL) was added to a 500 mL round bottom flask equipped with a stir bar, and the resulting mixture was stirred for 5 minutes at room temperature under argon. 6-bromohexane (6.55 mL, 46.6 mmol) was added via syringe and the mixture was stirred for 20 h at room temperature. After 20 h, the reaction mixture was poured into 40 mL of dichloromethane and washed with brine (3×50 mL). If the aqueous layer remained turbid after the third wash, 10 mL of DI water were added, and the mixture was extracted with dichloromethane. This process was repeated until the aqueous layer was colorless. The organic layers were combined, and the solvent was removed via rotary evaporation under reduced pressure. *N*-9 and *N*-7 substituted isomers were separated via flash column chromatography using dichloromethane with 1% methanol (by volume). The *N*-9 product was recovered at a 60% yield. ^{1}H NMR and ^{13}C NMR spectra were consistent with data previously reported by Sabury *et al*.[36]

Synthesis of 9-hexyl-2,6-bis(3-hexylthiophen-2-yl)-9*H*-purine (M1). An oven-dried 100 mL round bottom flask containing a stir bar was flushed with argon. After it cooled to ambient

temperature, 2,6-dichloro-9-hexyl-9*H*-purine (0.313 g, 1.15 mmol) and dried/degassed toluene (30 mL) were added to the flask. The catalyst, $Pd(PPh_3)_4$ (55.1 mg, 0.0476 mmol), was added, followed by 3-hexylthiophene-2-boronic acid pinacol ester (0.710 mL, 2.37 mmol). Then, 11 mL of a previously-sparged aqueous solution of K_2CO_3 (2 M) were added. The reaction mixture was placed in an oil bath that was preheated to 95 ºC. Conversion was monitored by TLC. After 48 h, the reaction flask was removed from the oil bath and allowed to cool to room temperature. Diethyl ether was added, and the mixture was extracted with brine (3×). The organic layers were combined, filtered, and dried. Flash column chromatography using a solvent mixture consisting of 1:3 ethyl acetate:hexanes was used to separate mono- and di-brominated products. The isolated yield of **M1** was 92%. ^{1}H and ^{13}C NMR spectra and the high-resolution mass spectrum (HRMS) are presented in the *Supporting Information* (**Figures S2**, **S3**, and **S6**). ^{1}H NMR (500 MHz, 25 °C, $CDCl_3$). δ, ppm: 0.88 (t, 6H, CH_3), 1.19-1.52 (m, 18H, CH_2), 1.75 (p, 4H, CH_2), 1.96 (p, 2H, CH_2), 3.31 (t, 2H, $ArCH_2$), 3.44 (t, 2H, $ArCH_2$), 4.28 (t, 2H, NCH_2), 7.00 (d, 1H, ArH), 7.09 (d, 1H, ArH), 7.31 (d, 1H, ArH), 7.54 (d, 1H, ArH), 8.02 (s, 1H, C8-H). HRMS: calc'd $[M+H^+]$: 537.3080, found: 537.2793.

Synthesis of 2,6-bis(5-bromo-3-hexylthiophen-2-yl)-9-hexyl-9*H*-purine (M2). 9-Hexyl-2,6-bis(3-hexylthiophen-2-yl)-9*H*-purine (0.316 g, 0.589 mmol) was added to a 25 mL round bottom flask along with tetrahydrofuran (10 mL) and glacial acetic acid (10 mL). The mixture was stirred at room temperature for 30 min. *N*-Bromosuccinimide (0.227 g, 1.27 mmol) was then added gradually over 5 min. The reaction conversion was monitored via TLC. After 16 h, the solvents were removed via rotary evaporation under reduced pressure. Flash column chromatography using a solvent mixture consisting of 1:1 ethyl acetate:hexanes was used to separate mono- and di-

brominated products. The di-brominated product was collected as a pale, yellow powder, and the isolated yield of **M2** was 43%. ^{1}H and ^{13}C NMR spectra and the HRMS spectrum are presented in the *Supporting Information* (**Figure S4**, **S5**, and **S7**). ^{1}H NMR (500 MHz, 25 °C, $CDCl_3$). δ, ppm: 0.89 (m, 6H, CH_3), 1.17-1.54 (m, 18H, CH_2), 1.70 (p, 4H, CH_2), 1.95 (p, 2H, CH_2), 3.24 (t, 2H, $ArCH_2$), 3.34 (t, 2H, $ArCH_2$), 4.24 (t, 2H, NCH_2), 6.95 (s, 1H, ArH), 7.05 (s, 1H, ArH), 8.01 (s, 1H, C8-H). HRMS: calc'd $[M+H^+]$: 693.1290, found: 693.0957.

General Procedure for Direct Arylation Polymerization of Comonomers. The purine-containing monomer (either **M1** or **M2**) and desired comonomer were added (in a 1:1 stoichiometric ratio, 0.15 mmol of each monomer) to a 25 mL round bottom flask equipped with a Teflon stir bar. All DArP reactions were performed in 5 mL of DMAc at 95 °C with 4-5 mol% $Pd(OAc)_2$ as the catalyst, 3.0 equiv. of K_2CO_3 as the base, and 0.3 equiv. of PivOH as the proton shuttle, which has proven to be effective at limiting defects in DArP of monomers based on 3-hexylthiophene.[37] All reagents were added under a positive pressure of argon. Dry DMAc was sparged with argon for 15 min before it was added to the reaction vessel. After 18 h, the reaction was cooled to room temperature and added dropwise to cold methanol (MeOH, ~50 mL) to precipitate the copolymer. To isolate the copolymer, the recovered solid precipitate was washed with methanol (25 mL × 3) and acetone (25 mL × 3), followed by centrifugation for 10 min after each wash. The final isolated and purified polymer was dried and collected as a solid powder. ^{1}H NMR spectra and GPC traces of the copolymers are presented in the *Supporting Information* (**Figure S9-13** and **Figures S14-19**, respectively).

Density Functional Theory (DFT) and Density Functional Theory Tight Binding (DFTB) Calculations. Density functional theory (DFT) and density functional tight binding (DFTB) calculations were used to evaluate the geometric and electronic structure of the TPT monomer **M1** and a tetramer of the resulting copolymer, **P1$_{TPT}$**. In addition, DFTB was used to compute geometric and electronic structure of all six purine-based conjugated polymers. For full DFT calculations, monomer **M1** was optimized at the m06-2X[38]/cc-pvdz and B3LYP[39]/cc-pvdz level, e.g., via hybrid and metafunctionals that include exact exchange, and we used B3LYP/6-31G* for the **P1$_{TPT}$** tetramer. For these calculations the NWChem suite of programs (version 7.0.2)[40] was used. DFTB was used for tetramers, as DFTB and the extended tight binding methods enables simulations of relatively large systems at a reasonable accuracy but considerably faster than typical ab initio DFT.[41] We used DFTB version 21.1 with the third-Order Parameterization for Organic and Biological Systems (3OB)[42] alongside dispersion corrections via the DFTD3 approach to compute the geometric structure and electronic structure of tetramers of each purine-containing copolymer. Geometry optimization was converged to a maximal force component of 0.0001 eV/Å using the conjugate gradient approach. As noted later, because the structure of **P1$_{TPT}$** obtained by DFT using B3LYP/6-31G* was similar to that obtained with DFTB and bandgaps tracked experimental results, full DFT calculations for the other tetramers were not pursued.

■ RESULTS AND DISCUSSION

*Synthesis of Monomer Triads **M1** and **M2**.* Based on insights from our prior work,[29] we hypothesized that cross-coupling polymerizations involving purines would benefit from monomer designs that feature efficient coupling sites of equal reactivity. For this reason, **M1** was synthesized from the dihalopurine, 2,6-dichloro-9-hexyl-9*H*-purine, by *N*-9-alkylation of 2,6-dichloropurine

according to previously reported methods,[36] followed by Suzuki-Miyaura cross-coupling between 3-hexylthiophene-2-boronic acid pinacol ester and 2,6-dichloro-9-hexyl-9*H*-purine. (See Scheme 1.) Based on previous studies of alternating copolymers containing terthiophene, hexyl side chains on the thiophene-purine-thiophene (TPT) triad were expected to enhance the solubility of the conjugated copolymer.[36] ^{1}H NMR spectroscopy confirmed coupling at both the 2- and 6-positions of the purine scaffold, respectively (**Figure S2**). After purification and isolation of **M1**, *N*-bromosuccinimide (NBS) was used to synthesize the dibromo-substituted monomer **M2**, as shown in Scheme 1, and functionalization was confirmed by ^{1}H NMR spectroscopy. Specifically, the spectrum of **M1** (**Figure 2**, bottom) shows two sets of doublets associated with the C-H bonds of the thienyl rings coupled at the C2 and C6 positions of the purine, as well as the singlet associated with the proton from C8 of the purine scaffold (δ = 8.03 ppm). After bromination, the four doublets are lost and replaced by two singlets, as seen in the spectrum for **M2** (**Figure 2**, top).

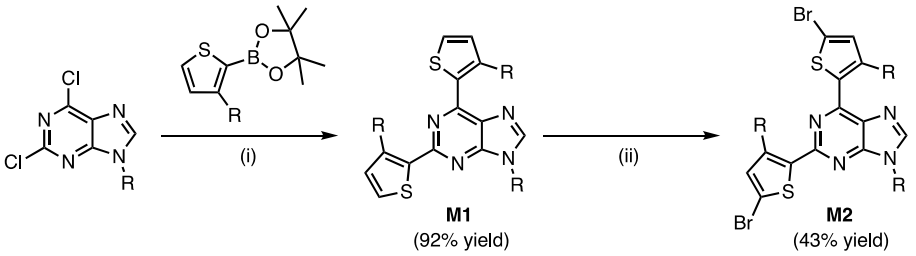

Scheme 1. Synthesis of thiophene-purine-thiophene triads, **M1** and **M2**, which have 2,6-connectivity due to the use of 2,6-dichloro-9-hexyl-9*H*-purine. R = hexyl. Synthetic conditions are (i) $Pd(PPh_3)_4$, 2 M K_2CO_3, toluene, reflux 110 °C for 48 h; (ii) 2 eq. NBS, THF/acetic acid, rt for 6 h.

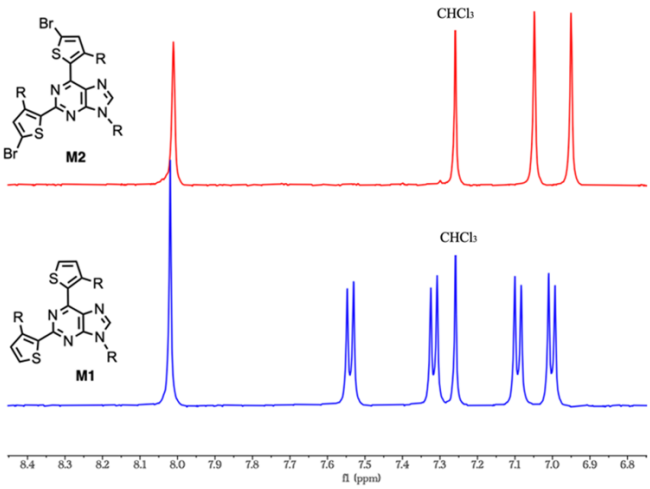

Figure 2. Aromatic region of the ^{1}H NMR spectra (in $CDCl_3$) confirming the selective conversion of **M1** (blue spectrum, bottom) to **M2 (**red spectrum, top) and retention of the proton at the purine C8 position. R = hexyl.

Synthesis of Purine-containing Copolymers. A series of fully conjugated, alternating copolymers containing the alkylated thiophene-purine-thiophene triads (**M1** or **M2**) were synthesized by DArP, as shown in Scheme 2. Two variations of AA + BB copolymerizations were used: First, **M1** was copolymerized with four different dibromo-monomers: **M2**, 2,5-dibromo-3-hexylthiophene (T), 4,7-bis(5-bromo-3-hexylthiophen-2-yl)benzo[*c*][1,2,5]thiadiazole (TBTT), or 2,7-dibromo-9,9-dioctyl-9*H*-fluorene (F). Second, the dibrominated triad **M2** was copolymerized with either 2,2'-(9,9-dioctyl-9*H*-fluorene-2,7-diyl)dithiophene (TFT) or 3,4-dihydro-2*H*-thieno[3,4-*b*][1,4]dioxepine (ProDOT). These polymerizations generated a series of alternating, purine-containing copolymers that are designated as **P1**$_{\mathbf{TPT}}$, **P2**$_{\mathbf{F}}$, **P4**$_{\mathbf{T}}$, **P6**$_{\mathbf{TBTT}}$ (Scheme 2a), and **P3**$_{\mathbf{TFT}}$ and **P5**$_{\mathbf{ProDOT}}$ (Scheme 2b), where the subscript designates the comonomer used. After each copolymerization, the resultant copolymer was precipitated into cold methanol and isolated after washing the recovered precipitate with methanol (×3) and acetone (×3), followed by centrifugation after each wash. Copolymers with number average molecular weights ranging from 4 – 18 kg/mol were synthesized with yields ranging from 42 – 86%, as reported in Table S1. The conditions used

for polymerization were selected based on a variety of studies in which the synthesis of poly(3-hexylthiophene) by DArP was optimized to avoid regioerrors (or "defects").[43–46] Specifically, Thompson *et al*, demonstrated that bulky carboxylic acids (such as PivOH) effectively reduce β-activation,[37] while our previous study shows that a reaction temperature of 95 °C avoids activation of the proton at C8 position of the purine and undesired C-H activation on thienyl monomers.[42] Because of the influence of molecular weight on polymer properties and as elaborated in the following section, we chose to focus characterization studies on purine-containing copolymers having M_n = 10 kg/mol (nominal value).

The macromolecular characteristics of this set of copolymers are summarized in Table 1, and their ^{1}H NMR spectra are presented in **Figures S8-S13**. All resonances show the broadening expected for polymers as well as the characteristic signature of the C8-H proton (at δ = 8.0 ppm). Consistent with our earlier reports,[29] the asymmetry of the TPT monomer naturally leads to the possibility of producing multiple different repeat unit configurations during polymerization. In addition and as seen in **Figure 2**, the protons of the alkylthiophenes flanking the purine are not magnetically equivalent, which would give rise to different end group signatures if TPT triads at chain ends are connected through the thienyl moiety attached at either C2 or C6 of the purine scaffold. As a result, the aromatic regions of the ^{1}H NMR spectra are complex, and attempts to identify defects in the primary structure, which typically occur in small proportion and, therefore, are already difficult to diagnose,[37,43–46,48] are made even more challenging in these purine-containing copolymers. However, the ^{1}H NMR spectra were analyzed to assess whether the C8-H proton of the purine is activated during DArP, which would produce undesired branching defects. This was accomplished by comparing the C8 proton integration to protons assigned to the first methylene of the alkyl chain attached at *N*-9 (at δ = 4.2 ppm). As observed from **Figures S8-S13**,

the C8-H appears to not undergo cross-coupling, at least within the limits of accuracy normally assigned to NMR (± 5%). This result is not unexpected, as small molecules studies by Hocek *et al*. demonstrated that harsh reaction conditions (DMF, 160 °C, 60 h) and excess haloarene were required for direct arylation of purines at C8 (provided the C6 and *N-9* positions were blocked).[49]

Table 1. Yield and macromolecular characteristics of purine-containing copolymers synthesized by DArP.

	Yield (%)	M_n (kg/mol)[a]	$Đ$	X_n[b]
P1$_{TPT}$	71%	9.0	2.2	9
P2$_{F}$	80%	9.4	1.9	10
P3$_{TFT}$	48%	12.1	3.2	11
P4$_{T}$	53%	9.8	1.7	14
P5$_{ProDOT}$	42%	9.8	2.1	13
P6$_{TBTT}$	47%	12.5	2.5	12

[a]Number-average molecular weights (M_n) were measured by GPC (mobile phase of THF at 25 °C) using universal calibration analysis based on polystyrene (PS) standards. [b]X_n is the average degree of polymerization based on M_n.

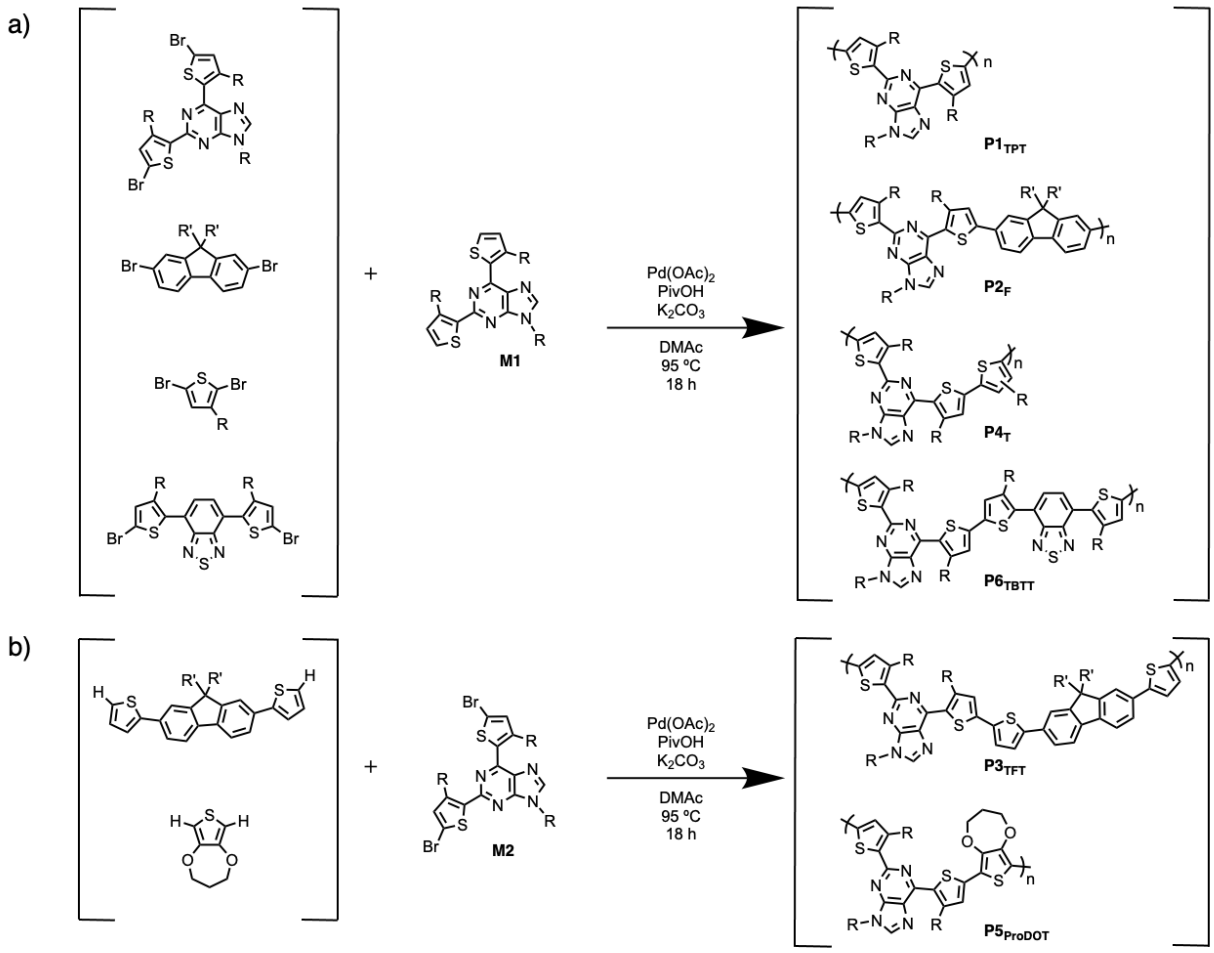

Scheme 2. Synthesis of purine-containing copolymers by DArP by copolymerization of a) **M1** with **M2**, F, T, or TBTT to form $\mathbf{P1_{TPT}}$, $\mathbf{P2_{F}}$, $\mathbf{P4_{T}}$, and $\mathbf{P6_{TBTT}}$, and of b) **M2** with TFT or ProDOT to form $\mathbf{P3_{TFT}}$ and $\mathbf{P5_{ProDOT}}$. In all structures, R = hexyl while R' = octyl.

Optical Properties of Copolymers. To investigate the dependence of optical properties on molecular weight, absorbance spectra were acquired for all copolymers. (See **Figures S20-S24** and Table S1 for data.) These studies provide some insight into the effective conjugation length (ECL) of these copolymers, as optoelectronic properties are expected to be independent of molecular weight above the ECL. For example, studies of oligothiophenes and poly(alkylthiophene)s showed that when the number of repeat units (N) in the chain exceeded 9-12 units, there were no observable changes in the absorbance spectrum.[50–53] Similarly,

homopolymers of 9,9-dialkyl-substituted fluorenes, which have a fused aromatic ring structure, have an effective conjugation length of 12 repeat units.[34,54] In both of these cases, the bulky alkyl side chains lead to out-of-plane deformation that reduce the conjugation length in comparison to highly planar polythiophenes, such as those made by Otsubo *et al*. They demonstrated that blocking β sites using a 2,2-bis(butoxymethyl)-1,3-propanediyl group allowed highly conjugated polythiophenes to be made, and those materials exhibited changes in optical absorption maxima up to chain lengths of N = 96.[55] Although our copolymers are disperse, the optical absorbance of our purine-containing copolymers becomes independent of molecular weight at $M_n \approx 9$ kg/mol. As an example, **Figure S23** shows that for **P4T**, there is a 5 nm red-shift in the absorbance maximum as the molecular weight is increased from 5.0 kg/mol (~7 repeat units) to 9.8 kg/mol (~14 repeat units); however, there are essentially no changes in the absorbance maxima and onsets as molecular weight is increased from 9.8 kg/mol to 18 kg/mol (~25 repeating units). The spectra of the other copolymers reflect the same pattern of behavior: There were no changes in absorbance maximum and onset above $M_n \approx 9$ kg/mol, which is reflected in absorbance maxima and onset values presented in Table S1. For this reason, optical and electronic properties reported in Table 2 were extracted from experiments that used copolymers where $M_n = 9.0 – 12.5$ kg/mol.

As shown in Table 2, the absorbance maximum (λ_{max}^{abs}) of all of the copolymers is between 400 – 460 nm, which is attributed to the π-π∗ transition.[56] Except for **P5ProDOT** and **P6TBTT**, broad and featureless absorbance spectra with $\lambda_{max}^{abs} \approx 420$ nm are observed. Relative to the other copolymers, **P5ProDOT** has a red-shifted absorbance maximum, which was expected due to the electron-rich nature of ProDOT and its high degree of planarity. **P6TBTT** has the most blue-shifted absorbance maximum ($\lambda_{max}^{abs} = 400$ nm) and the highest (bathochromic) absorbance onset ($\lambda_{onset}^{abs} = 569$ nm). The spectra of **P5ProDOT** and **P6TBTT** also exhibit distinctive shoulders or

secondary absorbance peaks at 500 and 463 nm, respectively, which could be attributed to ICT and indicative of a donor-acceptor relationship for these copolymers. A titration study using sequential additions of methanol to a chloroform solution of **P5$_{ProDOT}$** was completed to investigate whether the absorbance shoulder at 500 nm arose due to polymer aggregation. It is known that ProDOT homopolymers often exhibit dual-band absorbance profiles in solution caused by aggregation that is brought on by the planarity of the ProDOT monomer.[57] If the vibronic shoulder were a product of aggregation, an increase in the shoulder and a corresponding decrease in the main peak at λ= 458 nm with sequential additions of the poor solvent methanol would be expected. However, as seen in **Figure S32**, decreasing the solvent quality by adding methanol did not lead to an increase in the shoulder, which suggests that the shoulder in **P5$_{ProDOT}$** is not due to aggregation. Thus, this vibronic shoulder in the absorbance profile of **P5$_{ProDOT}$** is likely due to complementary S···O interactions that result in a more rigid backbone.[58] The absorbance maxima of **P6$_{TBTT}$** (400 nm and 463 nm) are similar to those reported previously for BT-containing chromophores[19,20] and alternating donor-acceptor copolymers where BT acts as the electron acceptor.[35,59] As discussed below, we hypothesize that this dual-band behavior arises due to ICT between the purine and the strong electron acceptor, BT.

Table 2. Optoelectronic data for purine-containing copolymers and **M1**.

	λ_{max}^{abs} [a]	λ_{onset}^{abs} [a]	λ_{max}^{em} [a]	λ_{onset}^{em} [a]	Stokes shift[a] (nm)	ϕ	Opt E_{gap}[b] (eV)
M1	309	377	405	488	96	0.12	--
P1$_{TPT}$	424	492	514	630	90	0.19	2.41
P2$_{F}$	416	479	475	606	59	0.61	2.46
P3$_{TFT}$	441	500	530	627	104	0.22	2.41
P4$_{T}$	426	514	515	637	98	0.17	2.24
P5$_{ProDOT}$	458	532	534	650	76	0.09	2.17
P6$_{TBTT}$	400	569	648	797	248	0.02	1.96

[a]UV-Vis and fluorescence spectra were acquired from $CHCl_3$ solutions. [b]Based on UV-Vis spectra acquired from drop cast thin films on glass slides.

Within this set of results, there are other aspects worth highlighting. For example, in comparison to **P1$_{TPT}$**, which is synthesized by an AA + BB copolymerization of **M1** and **M2**, the breadth of the absorbance peak of **P4$_{T}$** is larger while the absorbance maximum is basically unchanged. The differences in peak breadth may be attributed to **P4$_{T}$** being more flexible due to the additional hexylthiophene in the repeat unit, which provides more conformational freedom. This manifests as a broadening of the absorbance profile, which is a phenomenon that has been reported for other conjugated polymer systems.[60,61] Amongst the purine-containing copolymers, **P2$_{F}$** exhibits the highest onset energy (lowest λ_{onset}^{abs}) due to the high energy LUMO from the fluorene unit. The high energy onset of **P2$_{F}$** is similar to copolymers containing fluorene units in the main chain.[34,62,63] The absorbance data also show that when fluorene monomers are flanked with thiophenes (to create TFT) and then copolymerized with **M2** to produce **P3$_{TFT}$**, the absorbance onset and maximum are both lower in energy than **P2$_{F}$**. In addition to being soluble in chloroform, the purine-containing copolymers were soluble in tetrahydrofuran (THF) and *N,N*-dimethylformamide (DMF), which allowed solvatochromic properties to be examined in more polar solvents. (Adsorption spectra are presented in **Figures S33-S38**.) The absorbance profiles acquired for **P1$_{TPT}$** and **P4$_{T}$** show essentially no changes as solvent polarity is increased, while the λ_{onset}^{abs} of **P2$_{F}$**, **P5$_{ProDOT}$** and **P6$_{TBTT}$** are at lower energies in the most polar aprotic solvent, DMF. This change in λ_{onset}^{abs} is attributed to the excited state of **P2$_{F}$**, **P5$_{ProDOT}$**, and **P6$_{TBTT}$** being more polar than the ground state, and the polar solvent (DMF) assists in stabilization of the excited state.[64] **P3$_{TFT}$** exhibits a different pattern of behavior, showing a hypsochromic shift in λ_{onset}^{abs} and λ_{max}^{abs} with increasing solvent polarity, indicating a less polar excited state than ground state.[65]

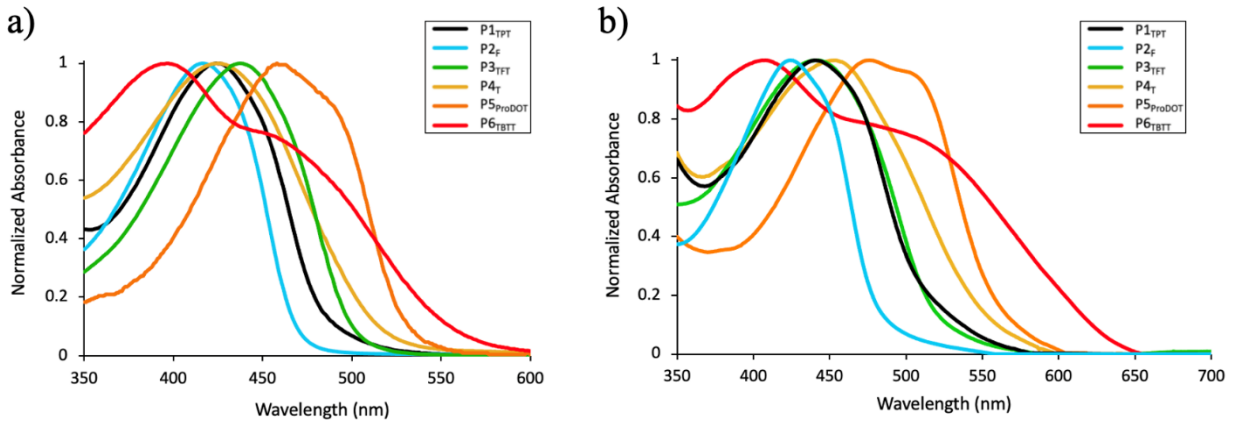

Figure 3. Normalized UV-Vis spectra for the various purine-containing copolymers: Spectra for **P1TPT** (black), **P2F** (blue), **P3TFT** (green), **P4T** (yellow), **P5ProDOT** (orange), and **P6TBTT** (red) were acquired a) at 0.01 mg/mL in $CHCl_3$ and b) as thin films.

To understand how optical properties change from solution to thin film, absorbance spectra were acquired from drop cast thin films, and are presented in **Figure 3b**. The absorbance maximum for films of **P6TBTT**, **P5ProDOT**, **P4T**, and **P1TPT** are red-shifted relative to those measured in chloroform ($CHCl_3$). This pattern of behavior is consistent with a larger degree of π-orbital overlap as well as a higher degree of ordering in the solid-state (as compared to solution-state measurements).[66] **P2F** showed no appreciable shift in absorbance maximum from solution to a thin film, ostensibly because the octyl groups on the sp^3-carbon of 9,9-dioctyl-9*H*-fluorene (F) disrupt packing in the solid state.[66,67] All of the purine-containing copolymers synthesized in this work are fluorescent, and as seen from **Figure 4**, they show visible emissions as solutions in $CHCl_3$, as thin films, and as powders. The emission spectra of the conjugated copolymers in $CHCl_3$ were measured by exciting at the λ_{max}^{abs} measured for each copolymer, and those values are tabulated in Table 2. As shown in **Figure 5**, the photoluminescence emission maximum and onset change significantly for each copolymer, with the emission spectrum of **P6TBTT** approaching the near-IR region of the electromagnetic spectrum. Compared to **P1TPT**, the fluorene-containing copolymer, **P2F**, has a hypsochromic shift, while **P4T**, **P5ProDOT**, and **P6TBTT** exhibit increasingly bathochromic

shifts. **P3$_{TFT}$** has the same absorbance maximum and onset as **P1$_{TPT}$** as thin films. While these traits are also reflected in the values of optical bandgap determined from the UV-Vis measurements (Table 2), it is not possible at this juncture to discern whether the pattern of behavior is due to solvatochromic effects, difference in stacking or organization due to inherent solubility of the chains, or a result of changes in conjugation. We note that both absorbance and emission patterns for **P6$_{TBTT}$** are consistent with previous reports of related small molecule chromophores.[19,20] Because **P6$_{TBTT}$** has dual-band character with localized maxima (red trace in **Figure 3a**), emission spectra were acquired at excitation wavelengths of 400 nm and 463 nm. Both excitation energies resulted in the same featureless emission spectra, which confirms ICT in **P6$_{TBTT}$**. The other purine-containing copolymers have fine-structure vibrational progressions in their emission spectra, which are consistent with the absence of ICT. **P1$_{TPT}$**, **P3$_{TFT}$**, and **P4$_{T}$** have emission maximums within 15 nm of each other and emission onsets within 10 nm of each other. (See **Figure 5** and Table 2.) **P6$_{TBTT}$**, which contains the strong electron acceptor BT, displays a large Stokes shift of 248 nm, which indicates a large degree of structural reorganization upon photoexcitation. The other copolymers show less structural reorganization, with Stokes shifts ranging from 59-104 nm.

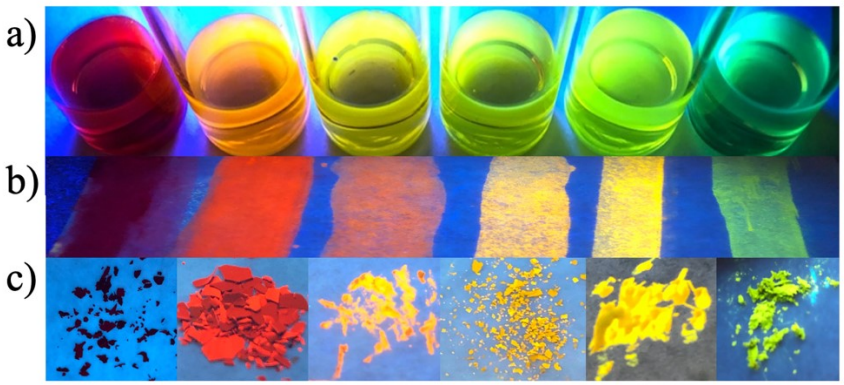

Figure 4. Images highlighting the emission behavior of purine-containing copolymers, from left to right, **P6$_{TBTT}$**, **P5$_{ProDOT}$**, **P4$_{T}$**, **P1$_{TPT}$**, **P3$_{TFT}$**, and **P2$_{F}$** in a) $CHCl_3$ solution at 1 mg/mL, b) the solid-state (thin films on wax paper), and c) as powders. Images were acquired by illuminating samples with a 365 nm UV lamp.

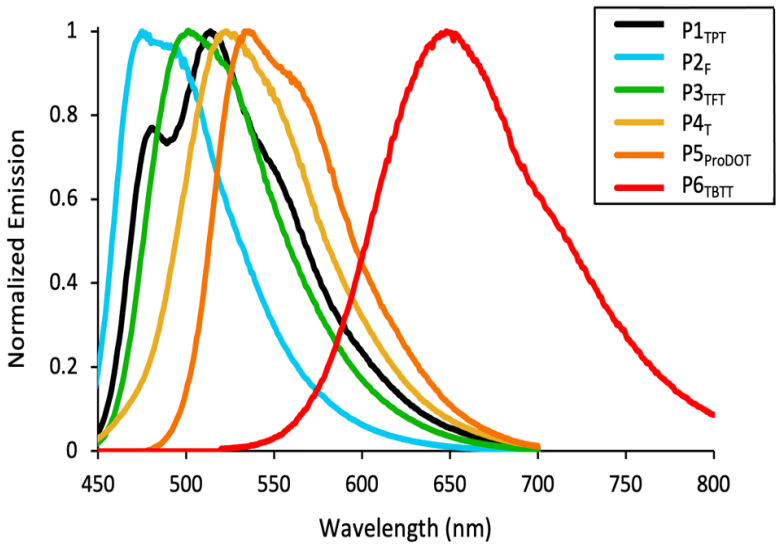

Figure 5. Normalized photoluminescence spectra of **P1**$_{\mathbf{TPT}}$ (black), **P2**$_{\mathbf{F}}$ (blue), **P3**$_{\mathbf{TFT}}$ (green), **P4**$_{\mathbf{T}}$ (yellow), **P5**$_{\mathbf{ProDOT}}$ (orange), and **P6**$_{\mathbf{TBTT}}$ (red). All emission spectra were acquired from chloroform solutions 0.001 mg/mL.

The extinction coefficient for each copolymer was determined from a series of absorption measurements at various concentrations, and the resulting Beer-Lambert plots are presented in **Figures S25-S31**. The fluorescence quantum yield (ϕ) was determined relative to Rhodamine 101 in ethanol (+0.01 wt.% HCl) by the comparative method.

$$\phi = \phi_r \left(\frac{m_s}{m_r}\right)\left(\frac{n_s}{n_r}\right)^2 \quad (1)$$

In this expression, m_s and m_r are the slopes of the lines relating integrated fluorescence and absorbance intensities, respectively, with subscripts *r* and *s* referring to the reference and sample, and n_s and n_r are the refractive indices of the sample and reference solvents, respectively. ϕ_r is the fractional quantum yield of the reference, Rhodamine 101 in ethanol, which has a $\phi_r = 1.00$.[68] As reflected in results presented in Table 2, the purine-containing copolymers exhibit quantum

yields that range widely, from $\phi = 0.02 – 0.61$. **M1** has a modest quantum yield of $\phi = 0.12$, which is lower than purine-containing chromophores reported in our previous study,[19] as well as those studied by Bou Zerdan *et al*.[20] Given that purines have vibrant photoemission characteristics, the lower quantum yield determined for **M1** may be the result of having only one purine unit in the structure, compared to small molecule chromophores capped at each end by a purine.[17,34] **P1$_{TPT}$** has a slightly higher quantum yield of $\phi = 0.19$, which is similar to that of copolymer **P4$_{T}$**, which has an additional thiophene interposed between the TPT triads. Most notably, **P2$_{F}$** has the highest fractional quantum yield at $\phi = 0.61$ while **P3$_{TFT}$** follows at $\phi = 0.22$, and these results are consistent with many studies demonstrating that small molecule chromophores and conjugated polymers containing fluorene are highly fluorescent.[16–20,24,25,69–71] These results also show that the increase in sulfur content from **P2$_{F}$** to **P3$_{TFT}$** leads to a decrease in fluorescence quantum yield, from $\phi = 0.61$ to $\phi = 0.22$, which is consistent with an internal heavy atom effect that facilitates intersystem crossing via spin orbit coupling.[72,73] Nevertheless, **P2$_{F}$** has a higher photoluminescent quantum yield than values reported for homopolymers of poly(alkylfluorene)s in chloroform[74] and a significantly higher quantum yield compared to thiophene-alkylfluorene copolymers,[75] suggesting that the purine unit contributes strongly to the highly fluorescent behavior. The quantum yields of these four purine-containing copolymers are notable, as a benchmark value of $\phi \geq 0.1$ is typically viewed as sufficient for use in organic light-emitting diodes and polymer dots.[76,77] Both **P5$_{ProDOT}$** and **P6$_{TBTT}$** have quantum yields below $\phi = 0.1$: **P5$_{ProDOT}$** has a modest quantum yield of $\phi = 0.09$ and **P6$_{TBTT}$** is significantly lower with a quantum yield of $\phi = 0.02$, which we hypothesize is due to non-radiative decay accompanying ICT.[78] While it is tempting to compare the quantum yield of these purine-containing copolymers against one another, it is

possible that the solvation state of each copolymer in chloroform is different, which brings solvation effects into play that are known to impact fluorescent emission.

Bandgaps, Orbital Energy Levels (HOMO-LUMO), and Structures. Oxidation and reduction behavior of the copolymers as thin films (created by drop-casting on a gold button electrode) were measured via cyclic voltammetry (CV). Oxidation and reduction onsets, E_{onset}^{ox} and E_{onset}^{red}, were used to estimate the HOMO and LUMO energy levels using Equations 2 and 3, respectively. Ferrocene was used as the reference and assuming that the Fc/Fc^{+} redox couple is 5.1 eV relative to a vacuum.[20,79,80]

$$E_{HOMO}\ (eV) = -(E_{onset}^{ox} + 5.1)\ eV \quad (2)$$

$$E_{LUMO}\ (eV) = -\left(E_{onset}^{red} + 5.1\right)\ eV \quad (3)$$

Cyclic voltammetry experiments show that **M1**, **P1$_{TPT}$**, **P3$_{TFT}$**, **P4$_{T}$**, **P5$_{ProDOT}$**, and **P6$_{TBTT}$** exhibit quasi-reversible oxidations within the acetonitrile solvent window (**Figures S39-S44**). The values of HOMO and LUMO for each polymer are tabulated in Table 3 and compared graphically in **Figure 6**. The redox onset potentials from CV were assigned from the intersection of the tangent line of the redox peak at half height to the baseline current, as has been described by Janssen *et al*.[81] Data for **P2$_{F}$** is not included because oxidation and reduction were not observed in the potential window of acetonitrile. Also, although the oxidation onset for **M1** was observed in CV, no reduction wave was observed. Thus, the LUMO for **M1** was calculated using the HOMO measured by CV and the optical bandgap (which was reported in Table 2). **P1$_{TPT}$** has a HOMO of -5.70 eV and a LUMO of -3.25 eV. When ProDOT is copolymerized (with **M2**), an increase in the

HOMO level is observed for **P5$_{ProDOT}$** (-5.39 eV) due to the electron-rich nature of ProDOT. The LUMO energy of **P5$_{ProDOT}$** (-3.14 eV) is similar to that of **P1$_{TPT}$** (-3.25 eV), which suggests that it is dictated primarily by the TPT triad. These frontier energy levels indicate a donor-acceptor relationship for **P5$_{ProDOT}$**, with the TPT unit serving as the electron acceptor and ProDOT functioning as the electron donor, which leads to an optical bandgap of 2.17 eV. **P6$_{TBTT}$** has the smallest optical bandgap of 1.96 eV and a low lying LUMO at -3.48 eV (compared to **P1$_{TPT}$**), suggesting a "weak donor-strong acceptor" relationship between the BT and purine-containing units. This character in which BT functions as the strong acceptor is consistent with the behavior reported for P-TBTT-P small molecule chromophores and corresponding DFT calculations.[19,20] These examples in which the purine unit acts either as the electron acceptor (i.e., **P5$_{ProDOT}$**) or as the electron donor (i.e., **P6$_{TBTT}$**) confirm the versatility of the purine monomer.[19,29] **P1$_{TPT}$**, **P3$_{TFT}$**, and **P4$_{T}$** all have bandgaps and molecular energy levels that suggest the comonomers TFT and T function as conjugated linkers between the aryl units of the main chain.

Table 3. Measured redox onsets and molecular energy levels for purine-containing copolymers and **M1**.

	Cyclic Voltammetry				**DFTB**	
	Oxidation Onset (V)	Reduction Onset (V)	HOMO (eV)	LUMO (eV)	HOMO (eV)	LUMO (eV)
M1	0.88	--[a]	-5.98	-2.70[b]	-5.32	-2.68
P1$_{TPT}$	0.60	-1.85	-5.70	-3.25	-4.77	-2.93
P2$_{F}$	--[a]	--[a]	--[a]	--[a]	-4.80	-2.79
P3$_{TFT}$	0.59	-2.16	-5.69	-2.94	-4.60	-2.92
P4$_{T}$	0.59	-1.81	-5.69	-3.29	-5.02	-3.34
P5$_{ProDOT}$	0.29	-1.96	-5.39	-3.14	-4.30	-2.79
P6$_{TBTT}$	0.50	-1.62	-5.60	-3.48	-4.35	-3.10

[a]Not measured because oxidation and reduction potentials were outside the potential window of acetonitrile. [b]Value is calculated based on the UV-Vis absorbance onset.

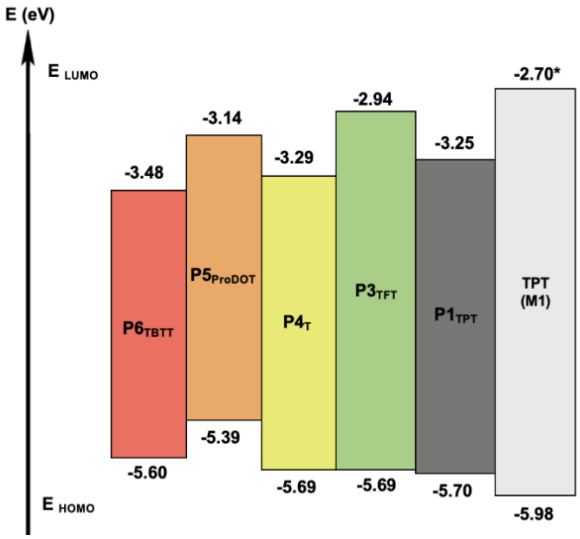

Figure 6. HOMO/LUMO energy level diagram of conjugated purine-containing copolymers obtained via cyclic voltammetry. The symbol * indicates that the LUMO for **M1** was calculated from the UV-Vis absorbance onset.

As shown in Table 3, trends in HOMO/LUMO energies derived from DFTB calculations generally agree with experimental results, even though calculations typically underestimate bandgaps and solvent was not considered. Frontier orbital energy levels computed for the tetramers of **P6$_{TBTT}$** and **P5$_{ProDOT}$** show the influence of the strong acceptor TBTT and strong donor ProDOT, and bandgaps increase from **P6$_{TBTT}$** to **P5$_{ProDOT}$** to **P4$_{T}$**. This pattern of behavior is also consistent with transition energies measured spectroscopically (Table 2). In addition, there is good agreement between energy levels calculated by DFTB and full DFT for **P1$_{TPT}$**. Full *ab initio* DFT calculations of **M1** at the B3LYP and m06-2X levels also show deep HOMOs and high LUMOs, which are consistent with those measured by cyclic voltammetry and computed by DFTB. (See Table S2 for comparisons of results obtained from DFT with different levels of theory and DFTB.) The optimized geometric structures obtained by DFT and by DFTB for **P1$_{TPT}$** tetramers are similar, as seen from structures presented in **Figure S45**, indicating reasonable accuracy of the tight

binding method. As noted earlier, because the tetramer structures obtained for **P1$_{TPT}$** with DFTB and with DFT are similar, we did not pursue full DFT calculations for the other copolymers. The optimized structures of **P1$_{TPT}$** also indicate that the **P1$_{TPT}$** tetramer is nearly planar – the largest dihedral variance along the **P1$_{TPT}$** tetramer backbone is 15°. Also, and as seen in **Figure S45**, **M1** shows a larger deviation from planarity because the thienyl group attached at C6 of the purine rotates out-of-plane by 30° while the flanking thienyl at C2 remains coplanar with the purine. (Dihedaral angle between them is within 10°.) (In addition to structures shown in **Figure S45**, XYZ files are included as *Supporting Information*.)

Finally, we would like to note the cross-conjugated nature of these copolymers, which arises because of the 2,6-pattern connectivity across the purine scaffold. As reported by Matsumoto *et al*.[82] and Janssen *et al*.[83] in their studies of donor-acceptor systems, cross-conjugation tends to weaken delocalization along the backbone, which lowers the HOMO energy. However, our TPT-based copolymers are different from typical alternating conjugated copolymers because **M1** and **M2** are comprised of triads that possess a cross-conjugated meta-linkage across the pyrimidine ring of the purine scaffold. Because of this design, a specific purine unit in the chain will have conjugated orbital overlap with one of the various comonomers used to construct the alternating copolymer, as evidenced by ICT observed for **P6$_{TBTT}$**. Although electronic communication throughout the main chain is likely weakened due to cross-conjugation, linearly conjugated subunits within the main chain consisting of P-T-comonomer-T-P units essentially act like oligomeric chromophores. Thus, these linearly conjugated, multi-ring subunits readily allow radiative decay, resulting in high quantum yields. This can be observed in the case of **P2$_{F}$**, where the copolymer benefits from the highly emissive nature of purines and fluorenes, and in the case of **P1$_{TPT}$** where the quantum yield of the copolymer is higher than its equivalent monomeric unit

even though the ratio of heavy atoms (thiophene-based units) is the same. Thus, while cross-conjugation is typically deleterious to optoelectronic properties, preserving electronic communication within a well-defined subunit of the chain appears to be a viable way to maintain properties and performance of conjugated polymers.

■ CONCLUSIONS

The synthesis and fundamental optoelectronic characteristics of fully conjugated copolymers incorporating 2,6-disubstituted purines in the main chain are described. Flanking the 2,6-dihalopurine with alkylthiophene units overcomes issues of unequal reactivity of coupling sites on the purine scaffold toward metal-mediated cross-coupling, allowing purine-containing copolymers with molecular weights up to 18 kg/mol to be synthesized by DArP. Naturally, the optical and electrochemical properties of these conjugated copolymers depend on comonomer selection, and this is also reflected in frontier orbital energy levels (HOMO/LUMO values) determined by cyclic voltammetry and through calculations based on density functional theory. Moreover, molecular orbital energy levels suggest that the TPT triad can participate as an electron-accepting unit in **P5**$_{\mathbf{ProDOT}}$ and as a donating unit in **P6**$_{\mathbf{TBTT}}$. Although the 2,6-connectivity across the pyrimidine ring of the purine results in cross-conjugation, these cross-conjugated designs with extended repeat unit structures are intriguing because of the possibility of tailoring electronic communication along the backbone. Finally, we note that the synthetic accessibility of specific sites on the purine scaffold enables design-structure-property relationships to be developed for other structural isomers, thereby engendering opportunities to enhance the properties of purine-containing conjugated materials.

■ Conflicts of interest

There are no conflicts to declare.

■ Acknowledgments

This work was sponsored in part by the U.S. Department of Energy's Office of Energy Efficiency and Renewable Energy (EERE) under the award number DE-EE0009177 provided to the University of Tennessee – Oak Ridge Innovation Institute (UT-ORII). SMK and BKL also acknowledge support from the National Science Foundation (Award # 2204396). CEO and SS acknowledge support in part from the UT-ORII Science Alliance Graduate Advancement, Training, and Education (GATE) program. Dr. Gabriel Goenaga is acknowledged with thanks for assistance with cyclic voltammetry measurements. DFT and DFTB calculations were performed at the Center for Nanophase Materials Sciences, a US Department of Energy Office of Science User Facility.

Abbreviation Table:

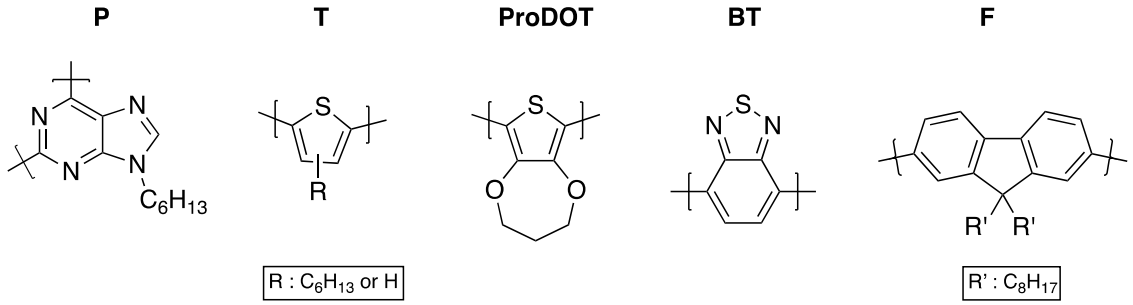

■ REFERENCES

1 M. Mondal, T. Begum and P. Bharali, *Catal. Sci. Technol.*, 2018, **8**, 6029–6056.
2 J. E. Šponer, Á. Vázquez-Mayagoitia, B. G. Sumpter, J. Leszczynski, J. Šponer, M. Otyepka, P. Banáš and M. Fuentes-Cabrera, *Chem. – Eur. J.*, 2010, **16**, 3057–3065.
3 M. Fuentes-Cabrera, B. G. Sumpter and J. C. Wells, *J. Phys. Chem. B*, 2005, **109**, 21135–21139.
4 Á. Vázquez-Mayagoitia, O. Huertas, G. Brancolini, A. Migliore, B. G. Sumpter, M. Orozco, F. J. Luque, R. Di Felice and M. Fuentes-Cabrera, *J. Phys. Chem. B*, 2009, **113**, 14465–14472.
5 M. Fuentes-Cabrera, B. G. Sumpter, P. Lipkowski and J. C. Wells, *J. Phys. Chem. B*, 2006, **110**, 6379–6384.
6 A. M. Martin, R. S. Butler, I. Ghiviriga, R. E. Giessert, K. A. Abboud and R. K. Castellano, *Chem. Commun.*, 2006, **42**, 4413–4415.
7 E. F. Gomez and A. J. Steckl, in *Green Materials for Electronics*, Wiley-VCH Verlag GmbH & Co. KGaA, Weinheim, Germany, 2017, 191–233.
8 T. Wang, R. Sha, R. Dreyfus, M. E. Leunissen, C. Maass, D. J. Pine, P. M. Chaikin and N. C. Seeman, *Nature*, 2011, **478**, 225–228.
9 N. C. Seeman, *Nature*, 2003, **421**, 427–431.
10 K. V. Gothelf and T. H. LaBean, *Org. Biomol. Chem.*, 2005, **3**, 4023–4037.
11 R. Lopez, Y.-J. Chen, S. Dumas Ang, S. Yekhanin, K. Makarychev, M. Z. Racz, G. Seelig, K. Strauss and L. Ceze, *Nat. Commun.*, 2019, **10**, 2933.
12 Y. Kang, A. Pitto-Barry, H. Willcock, W.-D. Quan, N. Kirby, A. M. Sanchez and R. K. O'Reilly, *Polym. Chem.*, 2015, **6**, 106–117.
13 P. Bäuerle and A. Emge, *Adv. Mater.*, 1998, **10**, 324–330.
14 S. Sivakova and S. J. Rowan, *Chem. Soc. Rev.*, 2005, **34**, 9.
15 S. Cheng, M. Zhang, N. Dixit, R. B. Moore and T. E. Long, *Macromolecules*, 2012, **45**, 805–812.
16 R. S. Butler, A. K. Myers, P. Bellarmine, K. A. Abboud and R. K. Castellano, *J. Mater. Chem.*, 2007, **17**, 1863–1865.
17 Y. Yang, P. Cohn, A. L. Dyer, S.-H. Eom, J. R. Reynolds, R. K. Castellano and J. Xue, *Chem. Mater.*, 2010, **22**, 3580–3582.
18 Y. Yang, P. Cohn, S.-H. Eom, K. A. Abboud, R. K. Castellano and J. Xue, *J. Mater. Chem. C*, 2013, **1**, 2867–2874.
19 G. S. Collier, L. A. Brown, E. S. Boone, M. Kaushal, M. N. Ericson, M. G. Walter, B. K. Long and S. M. Kilbey, *J. Mater. Chem. C*, 2017, **5**, 6891–6898.
20 R. Bou Zerdan, P. Cohn, E. Puodziukynaite, M. B. Baker, M. Voisin, C. Sarun and R. K. Castellano, *J. Org. Chem.*, 2015, **80**, 1828–1840.
21 L. H. Zucolotto Cocca, L. M. G. Abegão, L. F. Sciuti, R. Vabre, J. de Paula Siqueira, K. Kamada, C. R. Mendonca, S. Piguel and L. De Boni, *J. Phys. Chem. C*, 2020, **124**, 12617–12627.
22 K. Traskovskis, A. Sebris, I. Novosjolova, M. Turks, M. Guzauskas, D. Volyniuk, O. Bezvikonnyi, J. V. Grazulevicius, A. Mishnev, R. Grzibovskis and A. Vembris, *J. Mater. Chem. C*, 2021, **9**, 4532–4543.

23 A. Sebris, I. Novosjolova, K. Traskovskis, V. Kokars, N. Tetervenoka, A. Vembris and M. Turks, *ACS Omega*, 2022, **7**, 6, 5242–5253.
24 C.-C. Cheng, Y. Chu, F.-C. Chang, D.-J. Lee, Y.-C. Yen, J.-K. Chen, C. W. Chu and Z. Xin, *Nano Energy*, 2015, **13**, 1-8.
25 D. E. Fagnani, R. Bou Zerdan and R. K. Castellano, *J. Org. Chem.*, 2018, **83**, 12711–12721.
26 M. Hocek, *Eur. J. Org. Chem.*, 2003, **2003**, 245–254.
27 M. Havelková, D. Dvořák and M. Hocek, *Synthesis*, 2004, **2001**, 1704–1710.
28 I. Čerňa, R. Pohl, B. Klepetářová and M. Hocek, *J. Org. Chem.*, 2008, **73**, 9048–9054.
29 G. S. Collier, L. A. Brown, E. S. Boone, B. K. Long and S. M. Kilbey, *ACS Macro Lett.*, 2016, **5**, 682–687.
30 G. Langli, L.-L. Gundersen and F. Rise, *Tetrahedron*, 1996, **52**, 5625–5638.
31 T. A. Chen and R. D. Rieke, *J. Am. Chem. Soc.*, 1992, **114**, 10087–10088.
32 J. Lee, M. Jang, S. M. Lee, D. Yoo, T. J. Shin, J. H. Oh and C. Yang, *ACS Appl. Mater. Interfaces*, 2014, **6**, 20390–20399.
33 G. S. Collier, I. Pelse, A. M. Österholm and J. R. Reynolds, *Chem. Mater.*, 2018, **30**, 5161–5168.
34 A. R. Davis, J. J. Peterson and K. R. Carter, *ACS Macro Lett.*, 2012, **1**, 469–472.
35 P. M. Beaujuge, S. V. Vasilyeva, D. Y. Liu, S. Ellinger, T. D. McCarley and J. R. Reynolds, *Chem. Mater.*, 2012, **24**, 255–268.
36 S. Sabury, G. S. Collier, M. N. Ericson and S. M. Kilbey, *Polym. Chem.*, 2020, **11**, 820–829.
37 A. E. Rudenko, C. A. Wiley, J. F. Tannaci and B. C. Thompson, *J. Polym. Sci. Part Polym. Chem.*, 2013, **51**, 2660–2668.
38 Y. Zhao and D. G. Truhlar, *J. Chem. Phys.*, 2006, **125**, 194101.
39 A. D. Becke, *J. Chem. Phys.*, 1993, **98**, 5648–5652.
40 M. Valiev, E. J. Bylaska, N. Govind, K. Kowalski, T. P. Straatsma, H. J. J. Van Dam, D. Wang, J. Nieplocha, E. Apra, T. L. Windus and W. A. de Jong, *Comput. Phys. Commun.*, 2010, **181**, 1477–1489.
41 B. Hourahine, B. Aradi, V. Blum, F. Bonafé, A. Buccheri, C. Camacho, C. Cevallos, M. Y. Deshaye, T. Dumitrică, A. Dominguez, S. Ehlert, M. Elstner, T. van der Heide, J. Hermann, S. Irle, J. J. Kranz, C. Köhler, T. Kowalczyk, T. Kubař, I. S. Lee, V. Lutsker, R. J. Maurer, S. K. Min, I. Mitchell, C. Negre, T. A. Niehaus, A. M. N. Niklasson, A. J. Page, A. Pecchia, G. Penazzi, M. P. Persson, J. Řezáč, C. G. Sánchez, M. Sternberg, M. Stöhr, F. Stuckenberg, A. Tkatchenko, V. W. -z. Yu and T. Frauenheim, *J. Chem. Phys.*, 2020, **152**, 124101.
42 M. Gaus, A. Goez and M. Elstner, *J. Chem. Theory Comput.*, 2013, **9**, 338–354.
43 J.-R. Pouliot, F. Grenier, J. T. Blaskovits, S. Beaupré and M. Leclerc, *Chem. Rev.*, 2016, **116**, 14225–14274.
44 H. Bohra and M. Wang, *J. Mater. Chem. A*, 2017, **5**, 11550–11571.
45 S. Yu, F. Liu, J. Yu, S. Zhang, C. Cabanetos, Y. Gao and W. Huang, *J. Mater. Chem. C*, 2017, **5**, 29–40.
46 N. S. Gobalasingham and B. C. Thompson, *Prog. Polym. Sci.*, 2018, **83**, 135–201.
47 S. Sabury, B. LaRiviere, M. N. Ericson and S. M. Kilbey, *ACS Appl. Polym. Mater.*, 2021, **3**, 1012–1021.
48 A. E. Rudenko and B. C. Thompson, *J. Polym. Sci. Part Polym. Chem.*, 2015, **53**, 135–147.
49 I. Cerna, R. Pohl, B. Klepetarová and M. Hocek, *Org Lett*, 2006, **8**, 5389–5392.
50 J. Gierschner, J. Cornil and H.-J. Egelhaaf, *Adv. Mater.*, 2007, **19**, 173–191.

51 L. Zhang, N. S. Colella, B. P. Cherniawski, S. C. B. Mannsfeld and A. L. Briseno, *ACS Appl. Mater. Interfaces*, 2014, **6**, 5327–5343.
52 G. Bidan, A. De Nicola, V. Enée and S. Guillerez, *Chem. Mater.*, 1998, **10**, 1052–1058.
53 L. Zhang, N. S. Colella, F. Liu, S. Trahan, J. K. Baral, H. H. Winter, S. C. B. Mannsfeld and A. L. Briseno, *J. Am. Chem. Soc.*, 2013, **135**, 844–854.
54 G. Klaerner and R. D. Miller, *Macromolecules*, 1998, **31**, 2007–2009.
55 T. Izumi, S. Kobashi, K. Takimiya, Y. Aso and T. Otsubo, *J. Am. Chem. Soc.*, 2003, **125**, 5286–5287.
56 X. Liao, F. Wu, L. Zhang, L. Chen and Y. Chen, *Polym. Chem.*, 2015, **6**, 7726–7736.
57 A. M. Österholm, J. F. Ponder, M. De Keersmaecker, D. E. Shen and J. R. Reynolds, *Chem. Mater.*, 2019, **31**, 2971–2982.
58 C. B. Nielsen, A. Angerhofer, K. A. Abboud and J. R. Reynolds, *J. Am. Chem. Soc.*, 2008, **130**, 9734–9746.
59 A. Creamer, A. Casey, A. V. Marsh, M. Shahid, M. Gao and M. Heeney, *Macromolecules*, 2017, **50**, 2736–2746.
60 S. T. Hoffmann, H. Bässler and A. Köhler, *J. Phys. Chem. B*, 2010, **114**, 17037–17048.
61 M. J. Walter and J. M. Lupton, *Phys. Rev. Lett.*, 2009, **103**, 167401.
62 Z.-G. Zhang, K.-L. Zhang, G. Liu, C.-X. Zhu, K.-G. Neoh and E.-T. Kang, *Macromolecules*, 2009, **42**, 3104–3111.
63 B. Liu, W.-L. Yu, Y.-H. Lai and W. Huang, *Macromolecules*, 2000, **33**, 8945–8952.
64 A. A. Edwards and B. D. Alexander, in *Encyclopedia of Spectroscopy and Spectrometry*, Elsevier, 2010, 2030–2039.
65 S. Nigam and S. Rutan, *Appl. Spectrosc.*, 2001, **55**, 362A-370A.
66 S. H. Chen, H. L. Chou, A. C. Su and S. A. Chen, *Macromolecules*, 2004, **37**, 6833–6838.
67 S.-T. Huang, D.-J. Liaw, L.-G. Hsieh, C.-C. Chang, M.-K. Leung, K.-L. Wang, W.-T. Chen, K.-R. Lee, J.-Y. Lai, L.-H. Chan and C.-T. Chen, *J. Polym. Sci. Part Polym. Chem.*, 2009, **47**, 6231–6245.
68 T. Karstens and K. Kobs, *J. Phys. Chem.*, 1980, **84**, 1871–1872.
69 H. Kameshima, N. Nemoto and T. Endo, *J. Polym. Sci. Part Polym. Chem.*, 2001, **39**, 3143–3150.
70 T. Nakahama, D. Kitagawa, H. Sotome, S. Ito, H. Miyasaka and S. Kobatake, *Photochem. Photobiol. Sci.*, 2016, **15**, 1254–1263.
71 H. Kotaka, G. Konishi and K. Mizuno, *Tetrahedron Lett.*, 2010, **51**, 181–184.
72 S. C. Rasmussen, S. J. Evenson and C. B. McCausland, *Chem. Commun.*, 2015, **51**, 4528–4543.
73 B. Kraabel, D. Moses and A. J. Heeger, *J. Chem. Phys.*, 1995, **103**, 5102–5108.
74 H. P. M. Oliveira, T. D. Martins, K. M. Honório, P. C. Rodrigues, L. Akcelrud, A. B. F. Silva and T. D. Z. Atvars, *J. Braz. Chem. Soc.*, 2009, **20**, 160–166.
75 E. Ziegler, A. Pein, A. Fischereder and G. Trimmel, *Monatshefte Für Chem. - Chem. Mon.*, 2011, **142**, 193–200.
76 Z. Zhang, D. Chen, Z. Liu, D. Wang, J. Guo, J. Zheng, W. Qin and C. Wu, *ACS Appl. Polym. Mater.*, 2020, **2**, 74–79.
77 E. Ravindran and N. Somanathan, *J. Mater. Chem. C*, 2017, **5**, 4763–4774.
78 M. Bixon, J. Jortner, J. Cortes, H. Heitele and M. E. Michel-Beyerle, *J. Phys. Chem.*, 1994, **98**, 7289–7299.
79 L. Wen, C. L. Heth and S. C. Rasmussen, *Phys. Chem. Chem. Phys.*, 2014, **16**, 7231–7240.

80 B. C. Thompson, Y.-G. Kim, T. D. McCarley and J. R. Reynolds, *J. Am. Chem. Soc.*, 2006, **128**, 12714–12725.
81 R. E. M. Willems, C. H. L. Weijtens, X. de Vries, R. Coehoorn and R. A. J. Janssen, *Adv. Energy Mater.*, 2019, **9**, 1803677.
82 M. Ashizawa, T. Hasegawa, S. Kawauchi, H. Masunaga, T. Hikima, H. Sato and H. Matsumoto, *RSC Adv.*, 2016, **6**, 109434–109441.
83 G. W. P. van Pruissen, J. Brebels, K. H. Hendriks, M. M. Wienk and R. A. J. Janssen, *Macromolecules*, 2015, **48**, 2435–2443.

For Table of Contents Use Only

Highly Fluorescent Purine-Containing Conjugated Copolymers with Tailored Optoelectronic Properties

O'Connell *et al.*